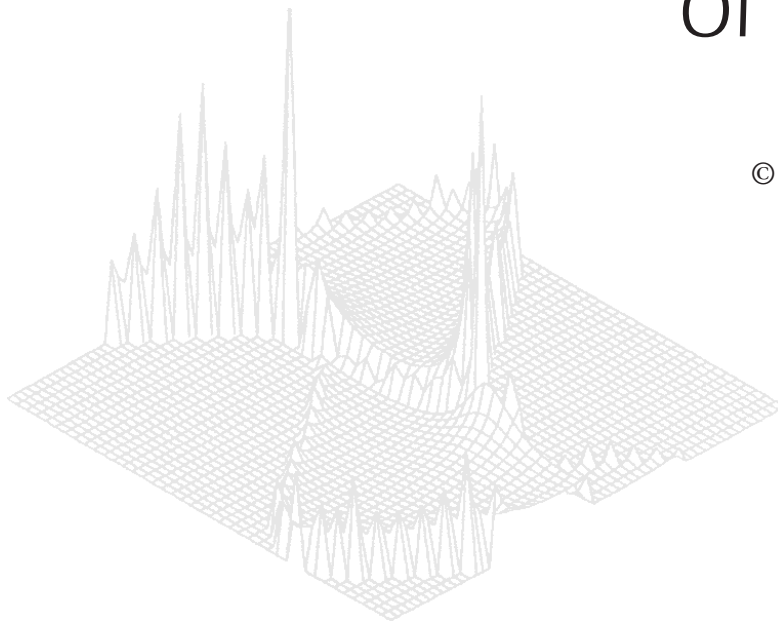

CSIRO PUBLISHING

Australian Journal of Physics

Volume 53, 2000
© CSIRO Australia 2000



A journal for the publication of
original research in all branches of physics

www.publish.csiro.au/journals/ajp

All enquiries and manuscripts should be directed to

Australian Journal of Physics

CSIRO PUBLISHING

PO Box 1139 (150 Oxford St)

Collingwood

Vic. 3066

Australia

Telephone: 61 3 9662 7626

Facsimile: 61 3 9662 7611

Email: peter.robertson@publish.csiro.au



Published by **CSIRO PUBLISHING**
for CSIRO Australia and
the Australian Academy of Science



Flux and Reactive Contributions to Electron Transport in Methane

K. F. Ness^A and A. M. Nolan^{B,C}

^A School of Mathematical and Physical Sciences,
James Cook University, Townsville, Qld 4811, Australia.

^B School of Chemistry, Physics and Earth Sciences,
Flinders University, GPO Box 2100,
Adelaide, SA 5001, Australia.

^C Present address: SOLA International Holdings Ltd,
Research & Development, PO Box 306,
Lonsdale, SA 5160, Australia.

Abstract

A previously developed theoretical analysis (Nolan *et al.* 1997) is applied to the study of electron transport in methane for reduced electric fields in the range 1 to 1000 Td. The technique of analysis identifies the flux and reactive components of the measurable transport, without resort to the two-term approximation. A comparison of the results of the Monte Carlo method with those of a multiterm Boltzmann equation analysis (Ness and Robson 1986) shows good agreement. The sensitivity of the modelled electron transport to post-ionisation energy partitioning is studied by comparison of three ionisation energy partitioning regimes at moderate (300 Td) and high (1000 Td) values of the reduced electric field.

1. Introduction

Electron transport in non-conservative (i.e. ionising and/or attaching) gases may be analysed in terms of flux and reactive components. The main motivation for such analysis is to gain insight into the effect of non-conservative processes on the electron transport. The details of this have been given in an earlier paper (Nolan *et al.* 1997). Here, for the sake of completeness, we give a brief outline.

In the hydrodynamic regime the measurable tensor transport coefficients include (Kumar *et al.* 1980)

$$\begin{aligned}
 \omega^{(0)} &\equiv \frac{d}{dt}(\log N) = \text{growth rate } (-\alpha), \\
 \omega^{(1)} &\equiv \frac{d}{dt}\langle \mathbf{r} \rangle = \text{drift velocity } (\mathbf{W}), \\
 \omega^{(2)} &\equiv \frac{1}{2!} \frac{d}{dt}\langle \mathbf{r}^* \mathbf{r}^* \rangle = \text{diffusion tensor } (\mathbf{D}), \\
 \omega^{(3)} &= \frac{1}{3!} \frac{d}{dt}\langle \mathbf{r}^* \mathbf{r}^* \mathbf{r}^* \rangle = \text{skew tensor}, \\
 \omega^{(4)} &= \frac{1}{4!} \frac{d}{dt}\langle \mathbf{r}^* \mathbf{r}^* \mathbf{r}^* \mathbf{r}^* \rangle = \text{kurtosis tensor}. \tag{1}
 \end{aligned}$$

Here the angular brackets $\langle \rangle$ denote ensemble averages in configuration space and $\mathbf{r}^* = \mathbf{r} - \langle \mathbf{r} \rangle$. These coefficients may be written in the form (Robson 1991)

$$\omega^{(k)} = \Gamma^{(k)} + S^{(k)}, \quad (2)$$

where $\Gamma^{(k)}$ represents the electron flux contribution to the observable transport, while $S^{(k)}$ is a source/sink term representing modification of the observable transport due to reactions involving the creation and/or loss of electrons. Assuming the case of an electric field only, directed in the $-z$ direction, the flux component of the drift velocity is denoted under this nomenclature as $\Gamma_z^{(1)}$ and the flux components of longitudinal and transverse diffusion are written as $\Gamma_{zz}^{(2)}$ and $\Gamma_{xx}^{(2)}$ respectively.

Even in the hydrodynamic regime the electron swarm energy distribution is normally spatially anisotropic. Electrons at the front of the swarm generally have higher energy than those at the rear, as they have been accelerated through a larger potential; see for example the analysis of Sugawara *et al.* (1998). If reactive collision channels exist which are energy dependent, the reactive processes will occur with a spatial dependence. For example, if there is an attachment process which occurs more readily at lower collision energies, it will naturally tend to occur at the rear of the swarm. Attachment loss of electrons from the rear of the swarm causes a forward shift to the swarm centre of mass, with a corresponding increase in the observable swarm drift velocity (Ness and Robson 1986; Sugawara *et al.* 1997). This change to the swarm centre of mass is the explicit effect of reactions, which is quantified by the S term in equation (2). There is also an implicit effect due to energy specific loss of electrons, which changes the swarm energy distribution as a whole, and thus indirectly changes the swarm flux Γ . It is not possible therefore to completely separate the effects of reactive collisions, except by analysis with and without the reactive interactions.

Nevertheless, the calculation of these so-called flux and reactive components does give an indication of the effect of non-conservative interactions upon electron transport. For example, if $S^{(k)}$ is small compared to $\Gamma^{(k)}$ then one can conclude that the effect of non-uniform creation/annihilation of electrons on the transport properties is small. On the other hand, having $S^{(k)}$ of comparable magnitude to $\Gamma^{(k)}$ would indicate a significant contribution of non-conservative interactions to the electron transport. Such knowledge may be important in the operation of gaseous electronic devices where electron transport through the gas plays an important role and one wishes to determine values of electric field strength and gas density for which ionisation may or may not have a significant effect on the drift and diffusion properties. In addition knowledge of the flux components of drift and diffusion is important in the fluid modelling of plasma discharges (White *et al.* 2000).

Methane provides an example of a gas which has application in a number of devices where the electron transport is important to the device behaviour. Such applications include drift chambers employed for the detection of high energy particles (Biagi 1989) and diffuse discharge switches for pulsed power applications (Christophorou *et al.* 1982; Schoenbach *et al.* 1982). Methane also has application in RF plasmas for the preparation of diamond-like or amorphous carbon thin films, where control of the film properties requires accurate knowledge of the electron transport (Yoshida *et al.* 1996).

Many approaches have been used to study the flux and reactive components of electron transport via Boltzmann analysis. Examples include the studies of Ségur and Bordage (1987), Robson and Ness (1986), Tagashira *et al.* (1977) and Taniguchi *et al.* (1977). The method by which one might study the problem via direct Monte Carlo simulation is not obvious; the approach of Blevin and Fletcher (1984), Blevin and Kelly (1991) and Brennan *et al.* (1990) was to apply a spatial gradient analysis to the electron swarm. This approach has been used here, but unlike these earlier works, the present technique does not resort to any two-term approximations in the analysis and therefore provides greater accuracy. This is demonstrated by the present application to the study of electron transport in methane, a problem which is notorious for failure of non-multiterm analyses (Haddad 1985; Ohmori *et al.* 1986; Schmidt 1991).

2. Calculations

The technique of analysis is described at length in Nolan *et al.* (1997) and requires the determination of the spatial variation of the swarm energy distribution. This is achieved during direct Monte Carlo simulation via summation of the electron spatial coordinates as a function of energy, with subsequent analysis occurring post-simulation. The flux component of the electron transport is calculated using the spatially dependent energy distributions. The observable electron transport may be determined by simple ensemble averages of the electron phase coordinates as per equation (1). The reactive component is the difference between these two quantities.

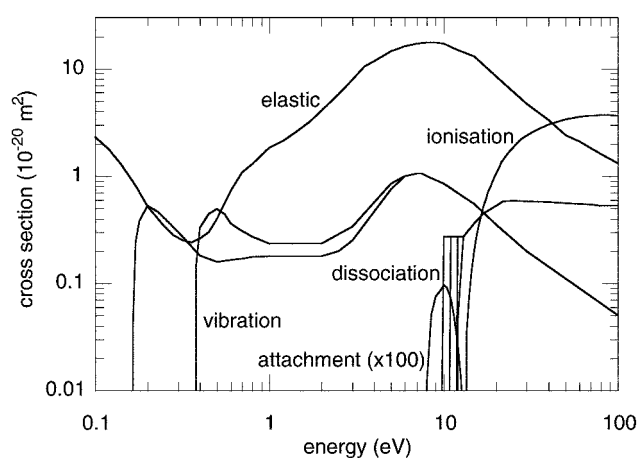


Fig. 1. Methane collision cross-section data.

This study considers electron transport in methane using the cross section set of Biagi (1989), which includes two vibrational channels, four dissociation channels, as well as elastic, ionisation and attachment channels. The cross-section data are shown in Fig. 1. Simulations have been performed for reduced electric fields (E/N) ranging from 1 to 1000 Td (note $1 \text{ Td} \equiv 10^{-21} \text{ V m}^{-2}$), with study of the electron transport in terms of the flux and reactive components.

Of separate interest is the influence of ionisation energy partitioning on the electron transport. In keeping with earlier studies by Ness and Robson (1986) and Tzeng and Kunhardt (1986), we have studied three distinct ionisation partitioning schemes. The different schemes allocate the available energy to the two post-collision electrons as follows:

- (1) a random fraction of the available energy is awarded to one electron, with the remaining energy awarded to the second electron.
- (2) the available energy is divided equally between the two electrons.
- (3) one electron receives all of the available energy, with the second electron having no initial energy.

The energy available for division after an ionising collision is given by the difference between the incident electron energy and the methane ionisation energy, here modelled as a constant 12.99 eV. Electron transport has been simulated using the three schemes outlined above for moderate (300 Td) and high (1000 Td) values of the reduced electric field.

The Monte Carlo simulations were simplified by assuming a stationary gas ($T = 0$ K), with the electron current assumed to be low enough for space charge effects to be negligible, allowing the swarm to be represented by an ensemble average of singly simulated electrons. To combat the computational overheads of modelling high ionisation rates at high E/N values, the simulations employed electron density scaling techniques similar to those used by Li *et al.* (1989).

To evaluate the accuracy of the Monte Carlo approach, Boltzmann analyses were performed in parallel with the Monte Carlo studies using the multiterm method described in detail by Ness and Robson (1986).

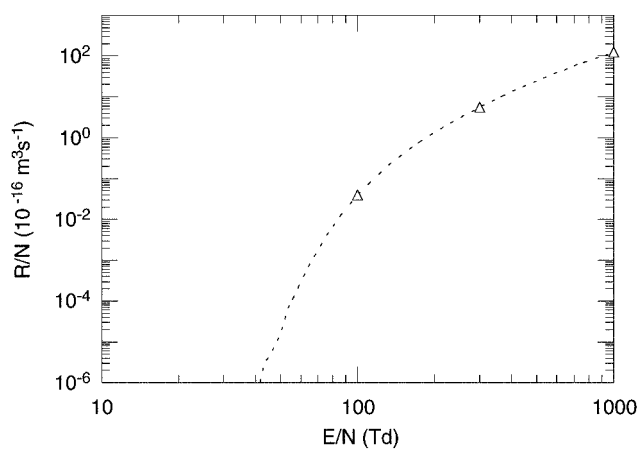


Fig. 2. Electron-methane reaction rate.

3. Results and Discussion

The flux and reactive components of various electron transport parameters are plotted in Figs 2–5 for reduced electric fields in the range 1 to 1000 Td. In these figures the data points represent Monte Carlo simulation results and the curves are the result of multiterm Boltzmann analysis. These data are for the random ionisation energy partitioning scheme. The reactive component of the electron

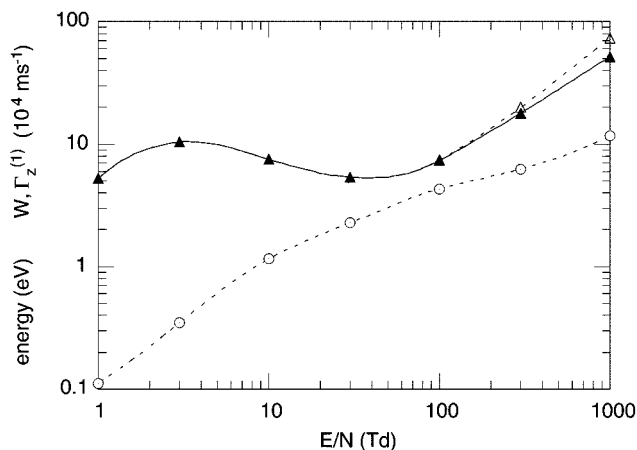


Fig. 3. Electron mean energy $\bar{\epsilon}$ (circles), drift velocity W (open triangles) and flux component $\Gamma_z^{(1)}$ (solid triangles).

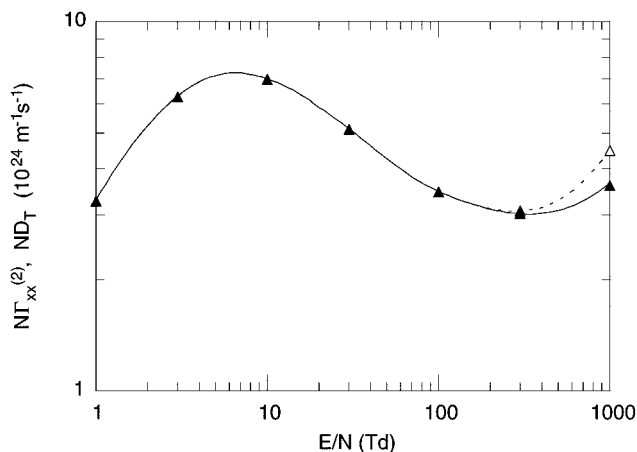


Fig. 4. Coefficient of transverse diffusion D_T (open triangles) and flux component $\Gamma_{xx}^{(2)}$ (solid triangles).

transport $S^{(k)}$ is given by the separation of the curves corresponding to the measurable electron transport and the flux component $\Gamma^{(k)}$. From these figures we see that the influence of reactions on the electron transport is not apparent until about 100 Td and increases with the electric field. This corresponds to an increase in the ionisation rate above this value of E/N ; the attachment rate was insignificant for all E/N studied.

These curves clearly demonstrate the explicit contribution of ionisation to the measurable electron transport in methane. The transport modification is a consequence of spatially non-uniform creation of ionisation progeny. Ionisation is most likely to occur at the front of an electron swarm where the higher energy electrons exist. Thus, in the case of drift (the centre-of-mass drift speed), ionisation acts to push the centre of mass of the swarm forward, increasing the

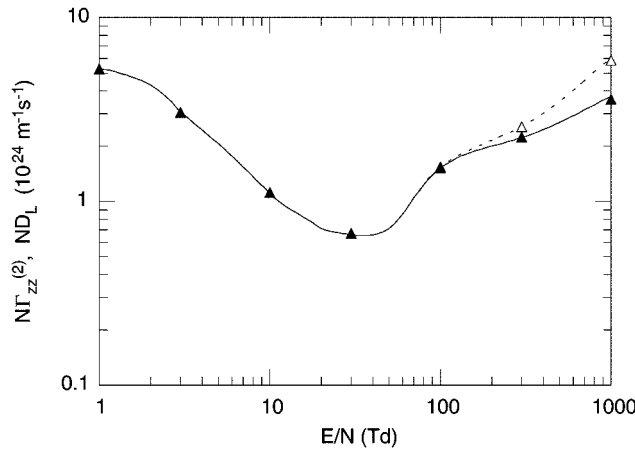


Fig. 5. Coefficient of longitudinal diffusion D_L (open triangles) and flux component $\Gamma_{zz}^{(2)}$ (solid triangles).

Table 1. Variation in electron transport coefficients with the ionisation energy partitioning

Simulations have been performed with random energy partitioning, equal energy partitioning and zero progeny energy. The terms in parentheses are the results of a multiterm Boltzmann analysis. Listed are the swarm mean energy $\bar{\epsilon}$, the reactive collision rate R/N and the measurable transport coefficients including the drift velocity W and the transverse and longitudinal diffusion coefficients D_L and D_T , expressed in terms of their flux and reactive components $\Gamma^{(k)}$ and $S^{(k)}$

Quantity		300 Td			1000 Td		
		Random	Equal	Zero	Random	Equal	Zero
W	(10^4 m s^{-1})	19.97 (19.99)	19.84 (19.85)	20.24 (20.25)	73.42 (73.43)	71.97 (72.02)	78.27 (78.30)
$\Gamma_z^{(1)}$	(10^4 m s^{-1})	17.94 (17.96)	17.84 (17.84)	18.16 (18.17)	51.90 (51.91)	50.97 (50.98)	54.91 (54.90)
$S_z^{(1)}$	(10^4 m s^{-1})	2.03 (2.03)	2.00 (2.01)	2.08 (2.08)	21.52 (21.52)	21.00 (21.04)	23.36 (23.40)
ND_T	$(10^{24} \text{ m}^{-1} \text{ s}^{-1})$	3.07 (3.072)	3.08 (3.077)	3.07 (3.059)	4.50 (4.50)	4.47 (4.46)	4.63 (4.65)
$N\Gamma_{xx}^{(2)}$	$(10^{24} \text{ m}^{-1} \text{ s}^{-1})$	3.02 (3.020)	3.01 (3.027)	3.01 (3.004)	3.68 (3.66)	3.70 (3.69)	3.55 (3.56)
$NS_{xx}^{(2)}$	$(10^{24} \text{ m}^{-1} \text{ s}^{-1})$	0.05 (0.052)	0.07 (0.050)	0.06 (0.055)	0.82 (0.84)	0.77 (0.77)	1.08 (1.09)
ND_L	$(10^{24} \text{ m}^{-1} \text{ s}^{-1})$	2.55 (2.561)	2.49 (2.495)	2.70 (2.69)	6.01 (6.03)	5.95 (5.95)	6.63 (6.64)
$N\Gamma_{zz}^{(2)}$	$(10^{24} \text{ m}^{-1} \text{ s}^{-1})$	2.23 (2.233)	2.16 (2.174)	2.36 (2.35)	3.73 (3.73)	3.66 (3.65)	4.28 (4.29)
$NS_{zz}^{(2)}$	$(10^{24} \text{ m}^{-1} \text{ s}^{-1})$	0.32 (0.328)	0.33 (0.321)	0.34 (0.34)	2.28 (2.30)	2.29 (2.30)	2.35 (2.35)
$\bar{\epsilon}$	(eV)	6.272 (6.272)	6.267 (6.267)	6.282 (6.282)	11.78 (11.78)	11.83 (11.83)	11.79 (11.79)
R/N	$(10^{-16} \text{ m}^3 \text{ s}^{-1})$	5.627 (5.630)	5.579 (5.582)	5.723 (5.728)	123.4 (123.4)	119.5 (119.5)	134.4 (134.2)

drift velocity W above its flux component $\Gamma_z^{(1)}$ (Ness and Robson 1986; Robson and Ness 1988; Sugawara *et al.* 1997). Note also that both diffusion coefficients are greater than their corresponding flux components. This indicates that the increase in electron numbers due to ionisation enhances diffusion in both parallel and perpendicular directions.

Table 1 lists the electron transport at 300 and 1000 Td, separated into the flux and reactive components, under the different ionisation energy partitioning schemes. Due to the technique of calculation of the various transport parameters (equation 1) the energy and reaction rate calculations have the least uncertainty and the diffusion coefficients the highest. This is reflected in the number of significant figures which are shown. The Boltzmann analysis calculates these parameters via a different means and is able to determine the electron diffusion to a higher certainty, except at high E/N where convergence in the Sonine polynomial expansion of the analysis becomes more difficult (Ness and Robson 1986).

When ionisation occurs, the total energy available to the two post-collision electrons for a given incident electron energy is the same independent of the way this energy is partitioned. The influence of the partitioning on the mean electron energy (and subsequently the transport coefficients) depends upon how fast the two electrons can gain energy from the applied electric field. For a given field strength and incident energy, this in turn depends upon the energy dependence of the collision cross sections and the velocities of the post-collision electrons.

For example, if the two-post collision electrons have energies such that they enter a region of low collision probability, this should lead to a higher mean energy than if one or both of the post-collision electrons are scattered into an energy region or regions of higher collision probability. In addition, on the microscopic level at least, the initial velocities of the two post-ionisation electrons affect their rate of energy gain from the applied field. For example, with the two electrons scattered in a direction opposite to the applied field, electrons with a 50:50 energy partition will together gain energy at a faster rate than if a 0:100 energy partition is applied. For scattering in the direction of the applied field the reverse applies. Here we have modelled isotropic scattering, where on average as many electrons are scattered in the direction of the field as against it. Hence this 'velocity effect' may have little influence, as the described microscopic behaviour would tend to average out for the swarm as a whole.

Referring to Table 1, at 300 Td the mean electron energy is approximately 6.3 eV and only a small fraction of electrons in the high energy tail of the swarm have sufficient energy to undergo ionising collisions (the threshold is 12.99 eV). This is indicated by the relatively low value of the ionisation rate R/N . For this value of E/N the 0:100 energy partitioning scheme gives the highest mean energy and, apart from transverse diffusion, the highest transport coefficients of the three partitioning schemes. At 1000 Td, where the mean energy is around 11.8 eV, a significantly larger fraction of the electrons in the swarm can undergo ionising collisions. In this case the highest mean energy occurs for the 50:50 energy partitioning scheme, while the drift velocity, longitudinal diffusion and reaction rate are maximised for the 0:100 energy partitioning scheme. This behaviour is related to the energy dependence of the elastic and the two vibrational cross sections in the region of zero to a few electron volts and the placement of the two post-ionisation electrons in energy space under the various partitioning schemes.

Recalling that the flux components of the transport coefficients can be expressed in terms of velocity integrals over the velocity distribution functions (Nolan *et al.* 1997), it follows that the variation in the $\Gamma^{(k)}$ with the partitioning of the post-ionisation energy indicates the influence of the energy partitioning schemes on the swarm velocity distribution functions. As expected this effect is more pronounced for the higher value of E/N as the ionisation rate is considerably higher.

The $S^{(k)}$ represent the explicit modification to swarm transport resulting from non-uniform creation and/or annihilation of swarm particles in space, due to energy dependent reactive collisions combined with a spatial variation of electron energies. For convenience we refer to the $S^{(k)}$ as the reactive components, although as seen above reactive interactions contribute to the flux component also: the so-called implicit effect (Robson and Ness 1988). If the reactive process is energy independent, then reactive interactions occur uniformly throughout the swarm so that the creation and/or annihilation of swarm particles neither enhances nor diminishes swarm transport: in this case all the $S^{(k)}$ vanish except for $S^{(0)}$ (the rate coefficient). Generally, reactive processes do have an energy dependence, as modelled here. The variation in the $S^{(k)}$ in Table 1 with the energy partitioning scheme indicates the explicit effect of the partitioning schemes on electron transport in methane due to the spatially non-uniform ionisation of methane molecules.

Different ionisation energy partitioning schemes will tend to scatter post-ionisation electrons into different energy regions in energy space with respect to the cross sections. This influences the mean energy and the collisional behaviour of the electrons, which in turn leads to variation in the transport coefficients with the partitioning scheme. Table 1 shows that in general the value of a given transport coefficient and that of its flux and reactive component (if applicable) for the random partitioning scheme lies between the values for the other two schemes. To a large extent this is to be expected as the equal energy and the zero energy schemes represent two ‘opposite’ extremes in the partitioning of post-ionisation energy.

For transport in this particular gas we observe that the longitudinal diffusion and drift velocity are more sensitive to variation in the ionisation energy partitioning than the transverse diffusion. Using the random energy partition scenario as a reference, at 1000 Td the percentage variations in the longitudinal diffusion and drift velocity under equal and zero energy partitioning schemes are over twice that of the variation in the transverse diffusion. This results from the lower sensitivity of the transverse diffusion coefficient to the cross sections in this energy region: comparison of Fig. 4 with Figs 3 and 5 shows that in the region of 1000 Td, D_T shows less variation with E/N than W and D_L . The large variation in the reaction rate under the different partitioning schemes observed at 1000 Td is due to the effect of the partitioning schemes on the population and energy distribution of electrons with sufficient energy to undergo ionisation and reflects the rapidly rising nature of the ionisation cross section above threshold.

The excellent agreement between all electron transport components calculated via Monte Carlo and Boltzmann techniques confirms the accuracy of this method of flux and reactive term analysis.

4. Conclusion

Swarm transport in conservative gases is purely a measure of the electron flux, while in non-conservative gases there may also be a contribution to measurable transport from the spatially anisotropic creation and/or loss of electrons. This latter contribution is termed the reactive component. The present study has confirmed the accuracy of a previously documented method for analysis of the flux and reactive components of electron transport in non-conservative gases via Monte Carlo analysis.

The energy dependence of the non-conservative collision channels in methane, combined with the natural spatial anisotropy of the hydrodynamic electron energy distribution, results in a reactive contribution to the electron transport. In the present study, ionisation collisions were observed to provide a noteworthy reactive contribution to swarm transport in methane at moderate to high values of E/N , while the insignificant rate of attachment provided no measurable effect.

Simulated electron transport in methane has been demonstrated as being sensitive to the choice of the ionisation energy partitioning model, particularly at high values of E/N , with the longitudinal transport coefficients being more sensitive to the partitioning choice than the transverse coefficients. This was explained in terms of the initial placement of the post-ionisation electrons in energy space with respect to the collision cross sections and the sensitivity of the various transport coefficients to the energy dependence of the cross sections.

At this stage the authors are unaware of any experiment that can separately measure the flux and reactive components of swarm transport when non-conservative interactions are present. If such experiments could be performed, their results would be of interest not only for the reasons already discussed in the Introduction, but also for their potential use in the determination and/or refinement of electron-neutral scattering cross sections based upon the inversion of swarm transport data (Crompton 1994). Further, such experiments might allow the ionisation energy partitioning function to be deduced by comparison of the measured transport components with simulated values over a range of E/N .

References

- Biagi, S. F. (1989). *Nucl. Instrum. Methods A* **283**, 716.
- Blevin, H. A., and Fletcher, J. (1984). *Aust. J. Phys.* **37**, 593.
- Blevin, H. A., and Kelly, L. J. (1991). In 'Gaseous Electronics and Its Applications' (Eds R. W. Crompton *et al.*), p. 127 (KTK Scientific: Tokyo).
- Brennan, M. J., Garvie, A. M., and Kelly, L. J. (1990). *Aust. J. Phys.* **43**, 27.
- Christophorou, L. G., Hunter, S. R., Carter, J. G., and Mathis, R. A. (1982). *Appl. Phys. Lett.* **41**, 147.
- Crompton, R. W. (1994). *Adv. At. Mol. Opt. Phys.* **32**, 97.
- Haddad, G. N. (1985). *Aust. J. Phys.* **38**, 677.
- Kumar, K., Skullerud, H. R., and Robson, R. E. (1980). *Aust. J. Phys.* **33**, 343.
- Li, Y. M., Pitchford, L. C., and Moratz, T. J. (1989). *Appl. Phys. Lett.* **54**, 1403.
- Ness, K. F., and Robson, R. E. (1986). *Phys. Rev. A* **34**, 2185.
- Nolan, A. M., Brennan, M. J., Ness, K. F., and Wedding, A. B. (1997). *J. Phys. D* **30**, 2865.
- Ohmori, Y., Kitamori, K., Shimoizuma, M., and Tagashira, H. (1986). *J. Phys. D* **19**, 437.
- Robson, R. E. (1991). *Aust. J. Phys.* **44**, 685.
- Robson, R. E., and Ness, K. F. (1986). *Phys. Rev. A* **33**, 2068.
- Robson, R. E., and Ness, K. F. (1988). *J. Chem. Phys.* **89**, 4815.
- Schmidt, B. (1991). *J. Phys. B* **24**, 4809.

- Schoenbach, K. H., Schaefer, G., Kristiansen, M., Hatfield, L. L., and Guenther, A. H. (1982). *IEEE Trans. Plasma Sci.* **PS-10**, 246.
- Ségur, P., and Bordage, M. C. (1987). XVIII Int. Conf. on Phenomena in Ionised Gases, Vol. 1 (Ed. W. T. Williams), p. 156 (Adam Hilger: Swansea).
- Sugawara, H., Sakai, Y., Tagashira, H., and Kitamori, K. (1998). *J. Phys. D* **31**, 319.
- Sugawara, H., Tagashira, H., and Sakai, Y. (1997). *J. Phys. D* **30**, 368.
- Tagashira, H., Sakai, Y., and Sakamoto, S. (1977). *J. Phys. D* **10**, 1051.
- Taniguchi, T., Tagashira, H., and Sakai, Y. (1977). *J. Phys. D* **10**, 2301.
- Tzeng, Y., and Kunhardt, E. E. (1986). *Phys. Rev. A* **34**, 2148.
- White, R. D., Robson, R. E., and Petrović, Z. Lj. (2000). in preparation.
- Yoshida, K., Ohshima, T., Ohmori, Y., Ohuchi, H., and Tagashira, H. (1996). *J. Phys. D* **29**, 1209.